Ultra-thin silver nanowires' synthesis in pore-confined space of mesoporous silica thin film

Magdalena Laskowska, Alain Walcarius, Andrii Fedorchuk, Maciej Zubko, Łukasz Laskowski

Available online at www.sciencedirect.com

jmr&t Journal of Materials Research and Technology

journal homepage: www.elsevier.com/locate/jmrt

Ultra-thin silver nanowires' synthesis in pore-confined space of mesoporous silica thin film

Magdalena Laskowska [a,b], *Alain Walcarius* [b], *Andrii Fedorchuk* [a], *Maciej Zubko* [c,d], *Łukasz Laskowski* [a,*]

[a] *Institute of Nuclear Physics Polish Academy of Sciences, Krakow PL-31342, Poland*
[b] *Université de Lorraine, CNRS, LCPME, Nancy F-54000, France*
[c] *Institute of Materials Engineering, Faculty of Science and Technology, University of Silesia, 75 Pułku Piechoty 1a, Chorzów 41-500, Poland*
[d] *Department of Physics, Faculty of Science, University of Hradec Králové, Rokitanského 62, Hradec Králové 500 03, Czech Republic*

ARTICLE INFO

Article history:
Received 23 February 2023
Accepted 3 May 2023
Available online 10 May 2023

Keywords:
Silver nanowires
Mesoporous silica films
Oriented nanopores
Nanoreactors
Electrode

ABSTRACT

In the present work, we report a synthesis procedure for the preparation of vertically aligned mesoporous silica thin films containing long, nanometer-scale thin silver nanowires inside pores. The inter-channel nanowires had a fine crystalline structure and a diameter of no more than 2 nm. Despite the diameter being the edge of the theoretical possibility of synthesis, the nanowires were stable enough to be observed by transmission electron microscope and could be clearly observed. For the synthesis, we applied the idea of silica nanoreactors, and the procedure consists of two steps: fabrication of an initial organically-functionalized silica thin film containing silver ions distributed regularly inside vertically aligned pores and following thermal decomposition resulting in the decomposition of the organic anchoring groups and the formation of metallic crystalline nanowires from released silver atoms. Both the final nanocomposite and the initial material were studied by means of transition electron microscopy and electrochemical techniques: linear scan and differential pulse anodic stripping voltammetry. The crystallinity of silver nanowires inside silica mesopores was proved by electron diffraction. The spatial confinement realized by silica nanochannels facilitated the stabilization of relatively small and ultra-thin nanowires and the formation of a hexagonal $P6_3/mmc$ silver crystalline structure instead of the more common $Fm3m$ cubic.

1. Introduction

Vertically aligned mesoporous silica thin film possesses an extraordinarily developed surface due to the presence of mesopores with great accessibility, which is one of the greatest advantages of such structures for practical applications [1–3]. They are typically prepared by electrochemically assisted self-assembly (EASA) [4,5], or via a Stöber-solution spontaneous growth procedure [6]. What is more, mesopores are uniformly, regularly, and 2D hexagonally distributed over

* Corresponding author.
E-mail address: lukasz.laskowski@ifj.edu.pl (Ł. Laskowski).
https://doi.org/10.1016/j.jmrt.2023.05.029

the whole underlying support, enabling easy access and fast transport of guest species through the membrane [2]. These properties also open a wide perspective for functionalization by grafting [7], or direct synthesis [8] methods. For both approaches, the precise control of the distribution of the inter-channels functional units is possible. In the case of grafting, the 2D solid solvent procedure can be applied [9]: a nanostructured material functionalized with both anchoring active groups and passive spacer groups, capable of selective ion or molecule capturing. Using such an approach, it is possible to obtain a material to adsorb a pre-defined amount of ions or molecules on its surface in such a way that functionalities are separated in space with a desirable average distance [10,11]. Direct synthesis, in turn, allows for the incorporation of the anchoring units directly during the synthesis of the host material without significantly narrowing the channels' volume [11], except when incorporating vast amounts of organo-functional groups [8].

Mesoporous silica films with perpendicularly oriented structures are basically of interest to be used as hard templates for the growth of nanowires, as done routinely with porous polycarbonate or alumina membranes [12,13], but their very narrow pore diameters (i.e., few nanometers [14]) may restrict the production of mechanically stable nanowires with ultra-small diameters [15]. Successful examples are macromolecular nanofilaments that were electropolymerized through such vertically aligned mesoporous silica thin films, as reported for polypyrrole [16], polythiophene [17], polyaniline [18], or polyquinone [19]. For metal electrodeposition, it is less straightforward [15], even if individual copper nanowires were electrochemically generated as single atomic switches through an oriented mesoporous silica membrane [20]. The electrochemical synthesis of quantum-dot arrays using mesoporous silica thin film as a template was also reported [21,22]. However, such metal-based 1D nanostructures are still rare.

The metal-containing molecules placed inside silica channels could be theoretically transformed into various types of nanoparticles or nanowires via various in-pore synthesis procedures [23]. In such a case, every individual pore would play the role of a separate nanoreactor, which could also provide space confinement. This later function would result in obtaining nanoparticles or nanowires with a predefined maximum size. The form of the structures appearing inside pores of the silica host should depend on the types of molecules bonded inside, their concentration, and the channels' geometry. Actually, mesoporous silica-based materials bearing organometallic moieties are very promising for applications in electrochemistry [24], or long-range charge transport [25], with possible use for next-generation electronics [26], and could also be exploited as hosts for the controlled generation of nanocrystals (known to be effective heterogeneous catalysts [27–29]). To reach this goal, there is a strong interest in developing novel methods from metallic nanoparticles or nanowires (either with magnetic or conductive materials likely to be used as superdense magnetic storage or supercapacitors [12]) as an alternative to electrodeposition approaches that might be limited for filling very small pores (even if electrochemical reduction of metal ions through vertically ordered mesoporous films is possible [30], but not giving always stable structures [15]). Let us consider silver: when it fills 2 nm mesopores oriented vertically to the conductive substrate, regularly and densely distributed, the obtained layout of highly conductive nanowires with a great specific surface area would be a promising material for supercapacitor's electrode [31,32].

In this article, we present such material: vertically aligned mesoporous silica containing ultra-thin and crystalline silver nanowires inside channels (see illustration in Fig. 1), which is produced by thermal decomposition of a silver complex anchored in the mesopore channels. The crystalline structure in the case of such thin (no more than 2 nm in diameter) silver wires is an extraordinary feature since such a diameter is a limit of the theoretical stability of the obtained ($P6_3/mmc$) crystalline structure [33]. The synthesis procedure presented here allows for the fabrication of such a unique nanocomposite.

2. Experimental

2.1. Materials synthesis

The fabrication of the materials involves two stages: (1) preparation of the initial materials, mesoporous silica thin films containing metal ions anchored inside the channels, followed by (2) their thermal decomposition, resulting in the creation of assumed nanostructures inside pores. The preparation of vertically aligned mesoporous silica thin films with silver nanoparticles inside pores (initial material) is based on our previous work [11] and is developed on electrochemically assisted co-condensation of tetraethyl orthosilicate (TEOS – Merck Ltd., Darmstadt, Germany) and 4- (triethoxysilyl)butyronitrile (BNTES – Merck Ltd., Darmstadt, Germany). In order to get silver-containing units as concentrated as possible in the material, we set the molar proportions between precursors as 4:1 TEOS:BNTES to reach a doping level of 20%, which is actually the largest one achievable for such EASA films without losing their ordered structure. The synthesis can be divided into the six main steps summarized in Fig. 2.

After this initial synthesis, we left a few samples for characterization, and the rest of the films were further processed via thermal treatment. As-synthesized silver-containing thin films were calcined at the temperature of 450°C for 3h in a protective atmosphere of nitrogen to obtain silver nanowires inside pores.

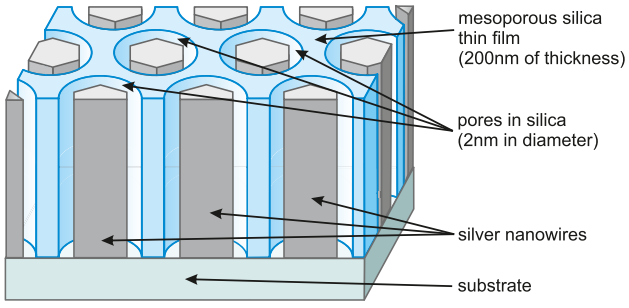

Fig. 1 – The schematic presentation of the experimental composite material: vertically aligned mesoporous silica containing crystalline silver nanowires inside channels.

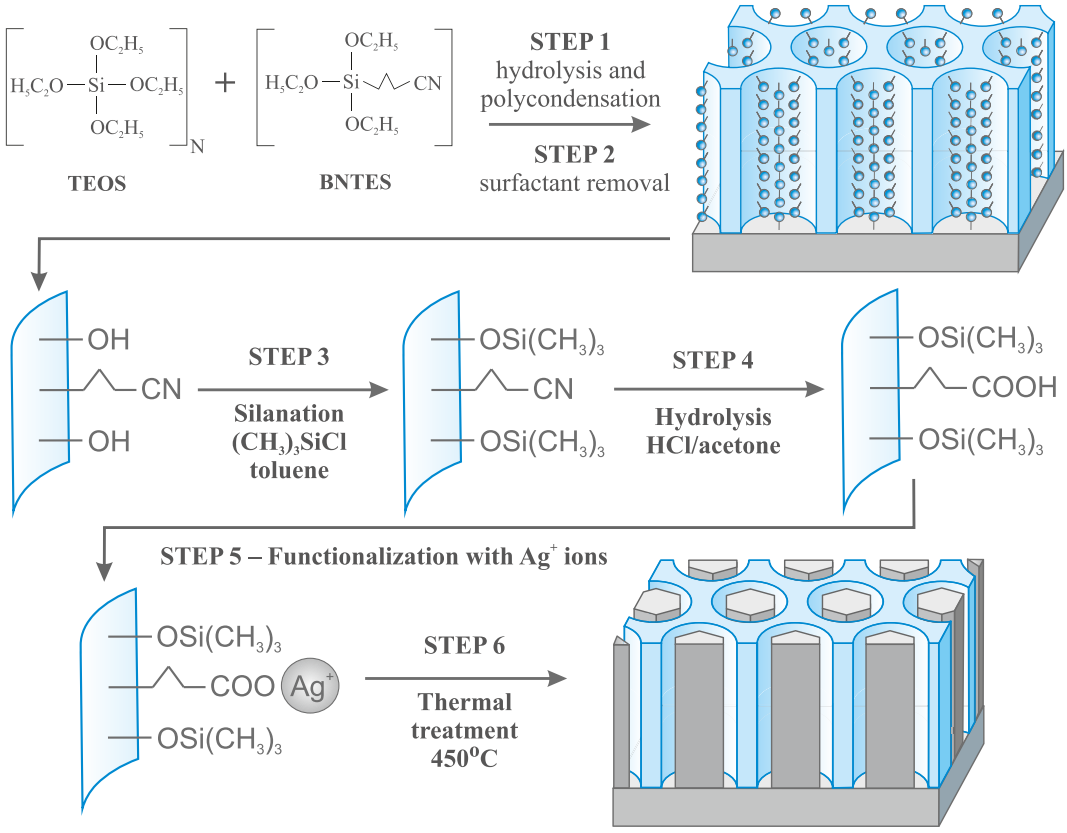

Fig. 2 – The general procedure of synthesis of 2D hexagonally arranged vertically aligned mesoporous silica thin films with pores containing silver nanoparticles inside pores. The number "N" determines the molar proportions between SiO_2 and functional silver-containing units. In this case, we set N = 4 in order to obtain a relatively high molar concentration of functionalities equal to 20%.

Summing up, we have obtained the following materials for further analysis.

- EASA-COOAg 4: mesoporous silica thin films containing silver ions in the molar concentration of 20% (with regards to SiO_2 molecules) - samples after the first stage of synthesis (before thermal processing)
- EASA-Ag NW: final samples: mesoporous silica thin films containing silver nanowires inside silica mesopores - samples after the second stage of synthesis (after thermal processing)

2.2. *Equipment and procedures*

The electrochemically-assisted self-assembly (chronoamperometry with the controlled potential of +1.5 V applied for 20 s) of vertically aligned mesoporous silica thin films was carried out using potentiostat/galvanostat SP150 (Biologic, France) at room temperature in the three-electrode system, in custom fabricated Teflon electrochemical cell. The working electrode on which the film was deposited was a conductive FTO-covered (fluorine-doped tin oxide) glass substrate (3D Nano Ltd., Poland). As the counter electrode, we used a platinum plate, and as the reference electrode - the standard Ag/AgCl electrode.

The same setup was used for the electrochemical analysis of obtained samples. The differential pulse anodic stripping voltammetry (DPASV) was carried out in order to investigate the efficiency of the functionalization procedure during the synthesis of the initial material, while the linear sweep voltammetry (LSV) was applied to the determination of the silver oxidation states in the initial (EASA-COOAg 4) and final (EASA-Ag NW) materials. Both measurements were carried out in 0.1M $NaNO_3$ electrolyte solution. For synthesis and electrochemical experiments, we used custom-fabricated Teflon cell, allowing for the application of the substrate at the bottom.

Raman spectra after each step of synthesis were recorded using a WITec confocal Raman microscope (CRM alpha 300) equipped with an air-cooled solid-state laser ($\lambda = 532$ nm) and a CCD camera. An air Olympus MPLAN (100 × /0.90 NA) lens was used. Raman scattered light was focused onto a multimode fiber and a monochromator with a 600 line per mm grating. The Raman spectra were accumulated by 10 scans with an integration time equal to 5 s and 3 cm^{-1} resolution. The spectra were collected at room temperature for the wavelength range of 100–4000 cm^{-1}. The baseline correction,

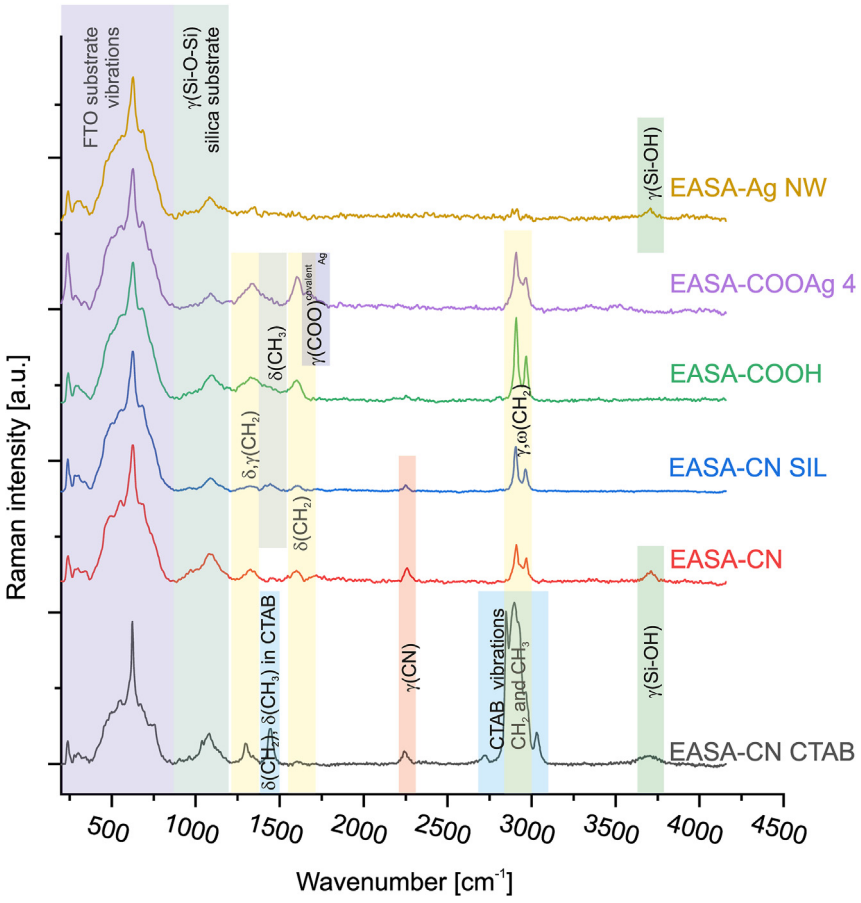

Fig. 3 – Raman spectra of the samples after each distinguish step of synthesis.

cosmic ray removal, and peak fitting analysis were performed using the WiTec Project software package.

The small angle X-ray diffraction (XRD) patterns of the functionalized silica films and calcined samples placed on a glass substrate were collected by means of Bruker D8 Advance diffractometer operated at 40 kV and 40 mA in inplane geometry (open Eulerian cradle (OEC)) with 80° Φ angle. CuKα radiation of wavelength 1.541Å and fixed slits were used. Scattering at a low-angle range of $1.5 \leq 2\theta \leq 8$ was recorded by applying 0.03 step size and 250s exposure time.

The TEM imaging of the obtained samples was carried out using a JEOL JEM-3010 high-resolution transmission electron microscope (TEM, JEOL Ltd., Tokyo, Japan) with 300 kV acceleration voltage, equipped with a LaB_6 emission source and Gatan 2k × 2k Orius^{TM} 833 SC200D CCD camera (Gatan Inc., Pleasanton, CA, USA). For fitting the electron diffraction patterns, we used Eldyf software (property of the Institute of Material Science of the University of Silesia).

Additional TEM images with a local EDS elemental analysis were gathered by the use of FEI Tecnai G2 20 X-TWIN electron microscope, equipped with emission source LaB_6, CCD camera FEI Eagle 2K, and X-Ray microanalyzer EDS.

The TEM images were processed using the Gwyddion software [34].

3. Results and discussion

Samples synthesis was monitored by Raman vibrational spectroscopy. The Raman spectra were collected after each step of the synthesis. The samples were labeled as follows to distinguish the curves on the graph.

- EASA-CN CTAB: materials after the first step of the synthesis, containing CTAB surfactant inside pores;
- EASA-CN: materials after the second step of the synthesis, surfactant washed out from pores;
- EASA-CN SIL: materials after the third step of the synthesis, silylated;
- EASA-COOH: materials after the fourth step of the synthesis, hydrolyzed;
- EASA-COOAg 4: materials after the fifth step of the synthesis, functionalized by silver;
- EASA-Ag NW: materials after the sixth step of the synthesis, thermally processed;

The juxtaposition of vibrational spectra, normalized to the highest peak at 629 cm^{-1}, can be seen in Fig. 3.

As can be seen, for all the samples, the first region to 950 cm^{-1} is dominated by a strong signal originating from the

FTO substrate [35], caused by the limitation of Raman depth resolution and small thickness of silica film. The next region (950–1250 cm^{-1}) is also strongly affected for the case of all the samples by silicon-oxide stretching vibration of the silica matrix [36,37]. The third, marked vibrational region (1200–1400 cm^{-1}), is common for most of the samples (with the exception of EASA-Ag NW) and is associated with vibrations of propyl chains in functional groups: scissoring and stretching of methyl [38,39]. The lack of these vibrations in the EASA-Ag NW sample is connected with the thermal decomposition of organic chains inside silica channels. The next feature connected with the symmetric stretching of methyl in propyl chains is also common for samples except for EASA-Ag NW and is located at 1600 cm^{-1} [40]. This peak is weak for the first material but still visible.

We will consider further vibrations with reference to specific samples. The first thin film, EASA-CN CTAB, shows a few characteristic features under vibrational spectroscopy. The first characteristic peak is visible at 1450 cm^{-1} and is associated with the deformation of methyl and methylene groups in CTAB surfactant, present in the silica pores [41].

The next characteristic band is centered at 2250 cm^{-1} and originates from C≡N and C–CN stretching [38,39,42]. Such vibrations can be observed for all non-hydrolyzed materials. A very broad and intense feature is located in the region from 2700 to 3100 cm^{-1}. All the peaks observed there are characteristic for the vibrations of CTAB surfactant: stretching of CH_2 groups and CH_3 headgroups in hexadecyl chains [41,43]. Such a broad band overlaps the peaks typical for vibrations of CH_2 groups in propyl chains located inside silica channels (clearly visible for further samples). Last characteristic peak, centered at 3690 cm^{-1}, takes from the Si–OH stretching mode [39,44]. Such surface hydroxyl units are present in non-silylated specimens only.

After washing off the CTAB surfactant from the silica pores, the Raman spectrum of the material changes in two regions. The first peak associated with CTAB at 1450 cm^{-1} disappears, similarly to the second, broad and intense feature at the region from 2700 to 3100 cm^{-1}. In this latter region, the vibrations originating from the propyl chains in functional units become apparent at the range from 2800 to 3000 cm^{-1}, which are associated with asymmetric and symmetric stretching vibrations and wagging of methylene CH_2 groups [40].

In the next step, materials were silylated, resulting in a substitution of the surface hydroxyl units by trimethyl silane units. Indeed, the peak at 3690 cm^{-1}, taken from the Si–OH stretching mode, disappeared in the sample EASA-CN SIL. Instead of this feature, one can note a subtle peak at 1450 cm^{-1} taken from the deformation of methyl units at trimethyl silane group [39,41,43].

Further functionalization of the samples implies the creation of silver carbonate molecules. Such moieties have characteristic vibrations mainly at the low wavenumber, in the region overlapped by FTO vibrations [45,46], however at the frequency about 1650 cm^{-1} one can observe a peak originates from asymmetric stretching of COO moieties with covalently bonded silver [46,47]. Indeed, such a peak can be observed in the spectrum of the EASA-COOAg 4 sample.

After the calcination, we expect the creation of metallic silver inside pores. None of the peaks originating from crystalline silver can be observed in the region of above 200 cm^{-1} [45,48,49]. The spectrum of the EASA-Ag NW sample indeed does not show any peaks that can prove metallic silver's presence. However, all the peaks originating from organic moieties disappeared. Based on this, it can be inferred that all anchor units were removed, and silver ions were released to form nanowires. The only new vibrational mode can be observed at 3690 cm^{-1}, taking from the Si–OH stretching mode [39,44]. Such a modification of the silica's surface is probably an effect of removing organic anchoring units and creating surface hydroxyl groups instead.

Just after the synthesis, we also carried out DPVAS measurements of the initial samples (EASA-COOAg 4) in order to further confirm the presence of the silver ions inside the silica channels. The typical DPASV result for the EASA-COOAg 4 is presented in Fig. 4. After electrolysis at 0.25 V for 1 min (leading to $Ag^{(I)}$ reduction into $Ag^{(0)}$ onto the electrode surface), one can see the presence of stripping peaks at approximately 0.2V corresponding to the reoxidation of silver deposits, the surface of which being proportional to the amount of electrochemically-accessible silver on the electrode [50]. We estimated the content of silver per single silica pore by carrying out a similar analysis as in our previous work [11] (see: Supplementary Information). Calculations have pointed out 116 ions per channel, but this value may be underestimated because some silver species can be not electrochemically accessible in such an insulating silica layer. Surely, it was the estimation of the lower limit of silver ions amount. Anyway, taking into consideration that the working solution contained no silver ions and this peak is absent for

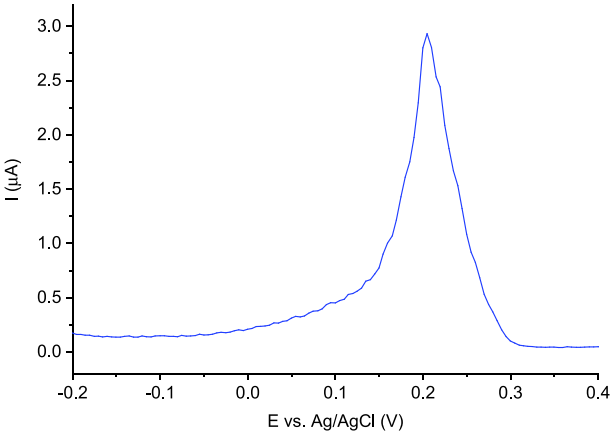

Fig. 4 – Differential pulse anodic stripping voltammetry (DPASV) curve recorded after 1 min electrolysis at −0.25 V in 0.1 M $NaNO_3$ electrolyte solution using silver-functionalized samples deposited on FTO-covered glass: vertically aligned porous silica thin film containing silver ions anchored via propyl-carboxylic units. Conditions of the experiment: pulse height of 2.5 mV, pulse width of 100 ms, step height of 5 mV, and step time of 500 ms.

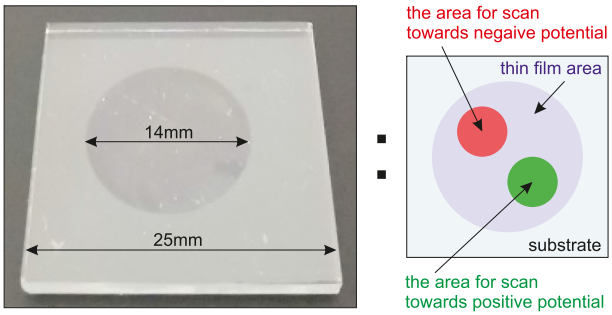

Fig. 5 – The appearance of the obtained thin silica films and the illustration of the areas used for the measuring of two linear scans on the same sample.

the non-activated films, the obtained result confirms the presence of silver-containing groups in the films.

In order to analyze the oxidation states of silver in both initial and final materials, we carried out linear scans of the materials both toward positive and negative potentials. The starting point of the scans was the equilibrium potential (zero-current potential) for the sample in the electrolyte solution, which was measured before the experiment.

In this experiment, if we detect the signal during scanning towards the cathodic (negative) direction, it would mean that the material contains some $Ag^{(I)}$ ions. When, in turn, the signal occurs during the anodic direction of the linear scan, it will indicate the presence of $Ag^{(0)}$ moieties.

The important is that both scans: toward positive and negative potential were done on the same sample, however, in different areas, as shown in the right part of Fig. 5. This can be achieved by the use of Teflon reactors with various bottom holes: a larger one for the preparation and a smaller one for electrochemical tests of obtained samples.

The results of the linear scans for both samples: initial (EASA-COOAg 4) and final (EASA-Ag NW), are shown in Fig. 6.

As can be clearly seen, the oxidation states of silver moieties are obviously different before and after the thermal treatment. Looking at the initial sample (EASA-COOAg 4 – Fig. 6 left plot), one can note a visible peak occurring during scanning towards the cathodic direction. No peak occurs during anodic scanning. This proves that the sample contains only $Ag^{(I)}$ ions (as expected). The opposite situation is demonstrated for the EASA-Ag NW sample. The cathodic scanning does not detect any signal, while it occurred during going towards the anodic direction, pointing out the presence of $Ag^{(0)}$ moieties only. This indicates that during the thermal processing of the samples, we deal with the transition of the $Ag^{(I)}$ ions (in the silver carbonate molecules) into metallic silver $Ag^{(0)}$.

After electrochemical tests, functionalized silica thin films were investigated using transmission electron microscopy in both imaging and diffraction modes. Especially later technique was essential for determining the nature of material inside mesopores. According to the assumption, the initially obtained silica thin films contain individual silver ions anchored by the carboxylate moieties and, therefore, amorphous. Thus, we should not observe any diffraction pattern. After thermal processing, however, the diffraction pattern can prove the creation of crystalline silver nanowires inside pores. Furthermore, the shape and location of silver nanowires can be easily determined using the bright field TEM mode.

Observation of the initial (non-calcinated samples – EASA-COOAg 4) has proven the silica's desirable mesopore structure, as shown in Fig. 7 (even if low magnification images show the presence of superimposed portions of the film because it was scratched from the electrode for analysis). Obtained silica thin films possess 2D hexagonally packed nanochannels aligned perpendicularly to the electrode's surface. Pore diameters can be estimated as 2 nm, and the interplanar distance can be estimated as about 3.5 nm. Additionally, we processed the TEM images using the 2D autocorrelation function (ACF) [34] to confirm the regular 2D hexagonal pore arrangement and find exact pore distribution parameters. As can be seen in Fig. 8, the parameters found on the basis of the ACF function are close to those observed directly in TEM images shown in Fig. 7. These observations are consistent with the previously

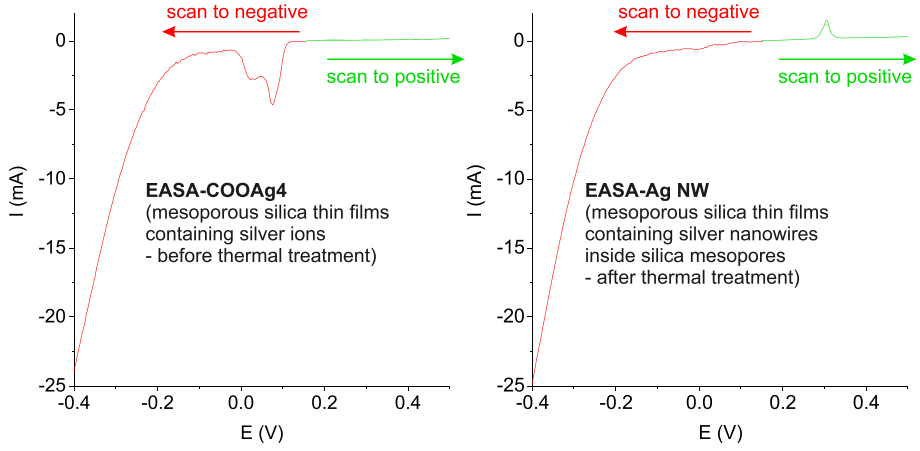

Fig. 6 – Linear scan voltammograms obtained for initial (EASA-COOAg 4) and final (EASA-Ag NW) materials in order to check the oxidation state of silver in both samples. Potentials were scanned from the equilibrium values (the potential at zero current), respectively, toward positive and negative values. Both measurements were performed on the different regions of samples (as in Fig. 5). The voltammograms have been recorded at a potential scan rate of 20 $mV \cdot s^{-1}$.

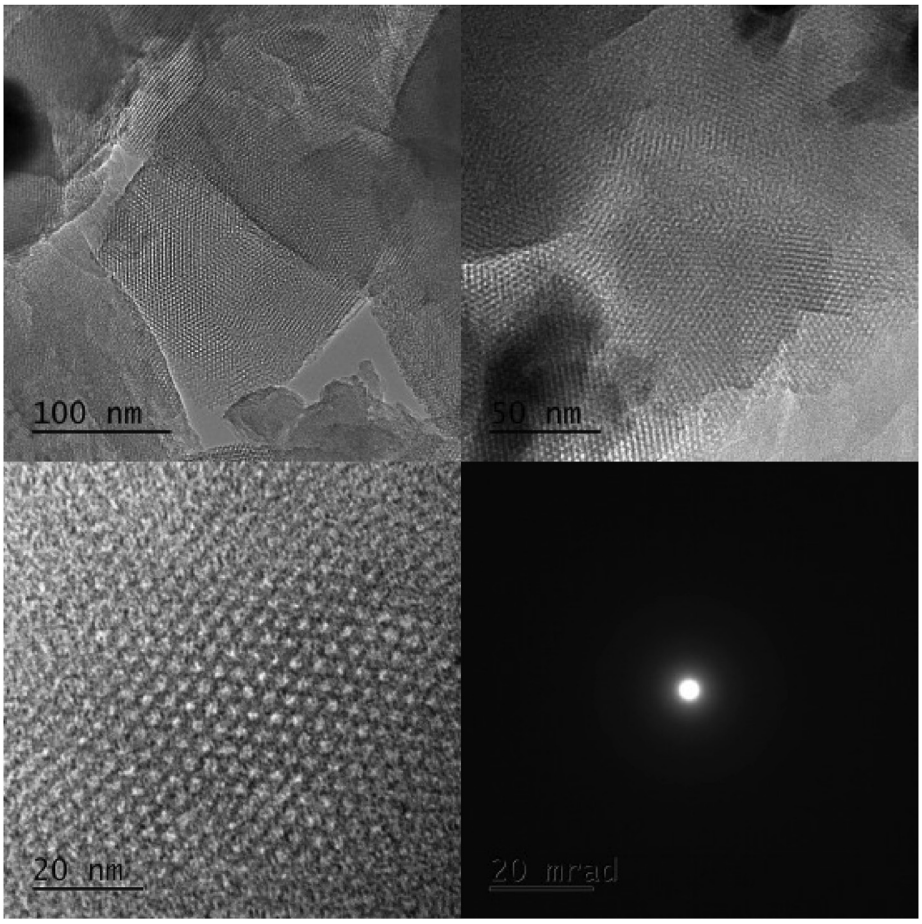

Fig. 7 – Transmission electron microscopy images of EASA-COOAg 4 sample together with electron diffractogram (right bottom image).

investigated mesoporous silica thin films prepared by EASA [4,5,8].

No solid particles nor impurities are visible in TEM images (Fig. 7). Also, no pattern from any possible crystalline structure can be observed on the electron diffractogram (Fig. 7 - right bottom image). Thus the sample is amorphous, consistent with the fact that silver ions are well-separated inside the silica matrix.

Along with TEM observation, samples were analyzed with regard to the atomic composition by the local EDS measurements (EDS analyzer incorporated in TEM microscope). Obtained electron dispersion spectra for EASA-COOAg 4 and

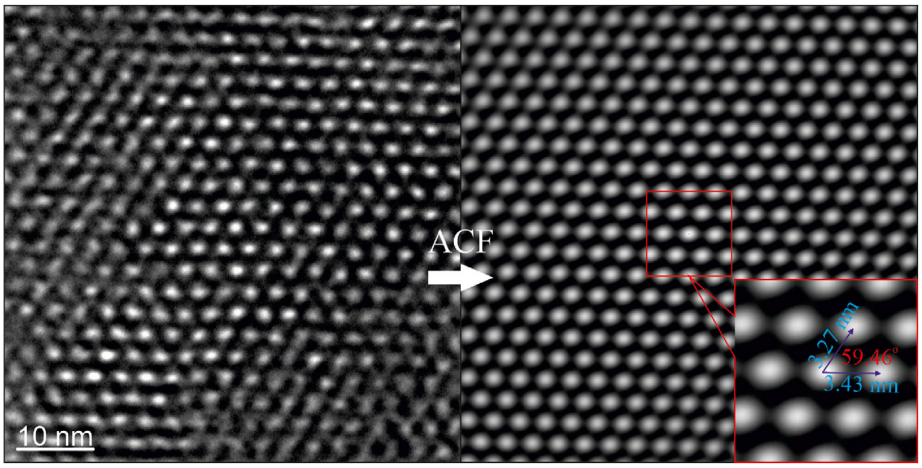

Fig. 8 – Transmission electron microscopy images of EASA-COOAg 4 sample (left) together with ACF processing of the sample's image (right) with marked elemental cell vectors and angle between them (inset).

Table 1 – The EDS quantification results for obtained thin films: EASA-COOAg 4, and EASA-Ag NW. The proportions between silicon and silver were normalized. EDS spectra were gathered from materials seen in Figs. 8 and 10.

Sample	Element	EDS quantification	
		mass [%]	molar [%]
EASA-COOAg 4	Si	45.625	76.318
	Ag	54.374	23.681
EASA-Ag NW	Si	43.831	75.038
	Ag	56.169	24.961

EASA-Ag NW can be found in Supplementary Materials, while the bulk content of silicon and silver were juxtaposed in Table 1.

From the synthesis conditions, we assumed 80% of silicon and 20% of silver (in molar proportions). The results presented in Table 1 indicated little higher silver amounts for both samples. The reason can be some additional number of silver ions physically adsorbed by the porous materials (instead of bounded by anchoring units). Nevertheless, the most important confirmation from EDS measurements is the presence of the silver species in the films without significant loss after thermal treatment.

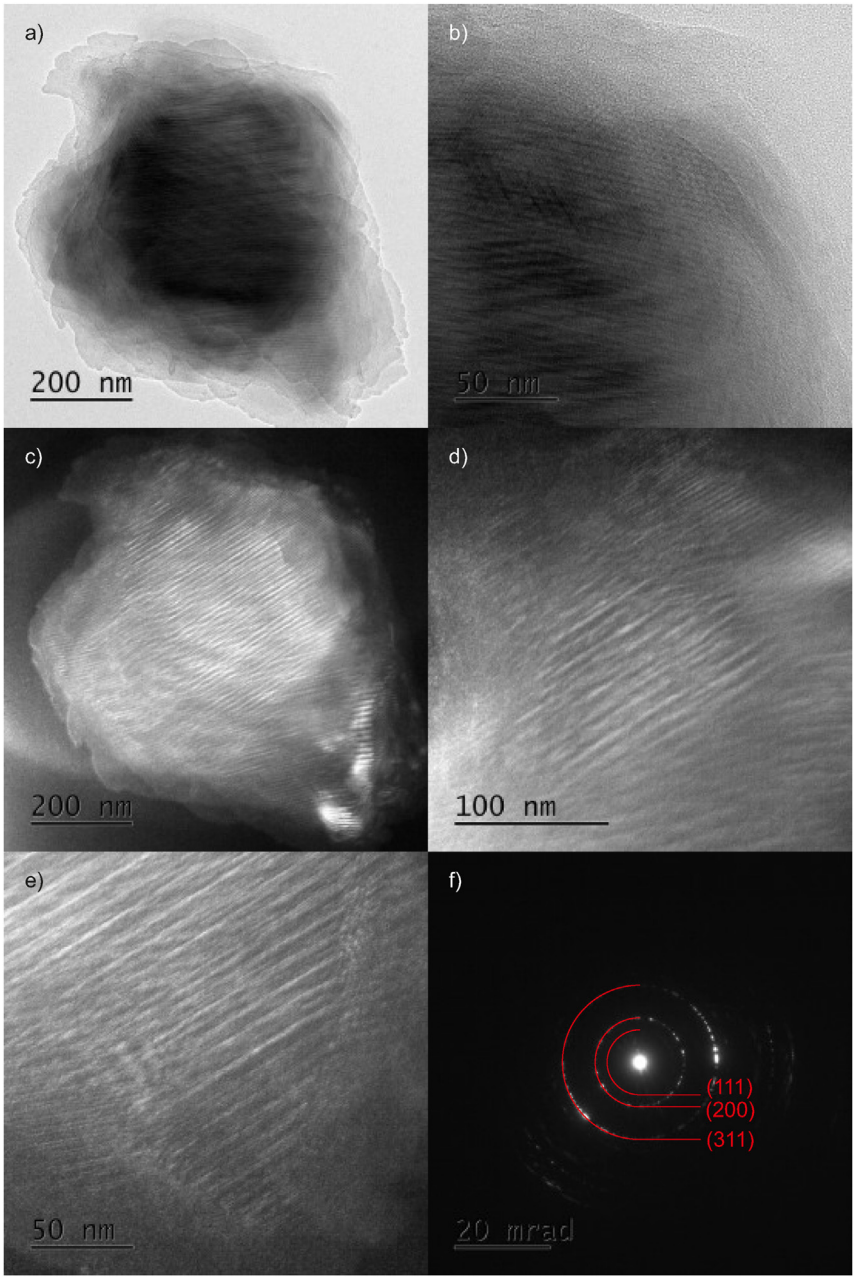

Fig. 9 – TEM images of the final material (EASA-Ag NW) containing silver nanowires. Images made in the bright (a,b) and dark (c–e) field, together with indexed selected area electron diffraction pattern (f).

After calcination of the initial sample (EASA-COOAg 4) at 450°C, its structure has changed significantly. As can be clearly seen in Fig. 9, instead of silica channels, one can clearly observe some nanowires placed inside (see also EDS results described further). Their arrangement fully corresponds to the 2D hexagonal arrangement of the silica channels in the EASA-COOAg 4. The distance between centers of individual nanowires can be estimated as 3–3.5 nm, thus similar to the case of the initial material. Looking at the TEM images, especially done in a bright field (9c-e), the diameter of visible nanowires seems to be no more than 2 nm. All these facts seem to prove that the nanowires have been created inside silica nanochannels.

The only possible material is silver, which has been released from the silver carbonate molecules attached inside silica channels after the thermal decomposition of organic groups. It seems to be confirmed by the EDS results juxtaposed in Table 1 (full EDS spectra can be found in Supplementary Materials).

What is more, the structure of silver nanowires is crystalline, as confirmed by the electron diffraction measurements, shown in Fig. 9f. After indexing, the obtained diffraction rings can be associated with the hexagonal $P6_3/mmc$ structure of silver [51]. The nanowires' length is difficult to estimate since we could not find any undamaged cross-section part of the sample. From the estimated amount of silver species in the film, they probably fill only partially the microchannels, which is, as such, already an extraordinary result.

Additional TEM observations resulted in finding a small part of the material with channels oriented almost perpendicularly to the observation's plane (Fig. 10, especially the right, upper part). We must emphasize that finding such a piece was not easy. Probably due to interchannel silver structures, which reinforced the material along the pores, making the material break more easily in that direction. Having imaged the mentioned part of the material, we applied the 2D autocorrelation function to find pores arrangement parameters. As shown in Fig. 10, the arrangement of the interchannel wires seems to be hexagonal. The length of the lattice vectors was not equal, but this may be due to the perspective of observation–the plane of the surface of the materials was not quite perpendicular to the direction of observation. The same may have caused the angle between the vectors to deviate from 60°. It is important that interchannel distances seem to be smaller than in the case of the EASA-COOAg 4 sample. It could be an effect of the material's shrinking during calcination. Such an effect can also be observed in XRD measurements, described further on.

Considering the diameter of silver nanowires of no more than 2 nm (silver structures are placed inside silica channels with the diameter of 2 nm), such structures are on the edge of the theoretical possibility of synthesis since, according to the calculations, particles smaller than 2 nm are not-stable [33]. However, in our case, the nanowires seemed to be stable since we did not notice any degradation under the electron beam, and the sample could be observed for a long time with no loss in the structure. It is probably a result of the using silica nanoreactors both as a synthesis environment and as a template for metallic nanowires.

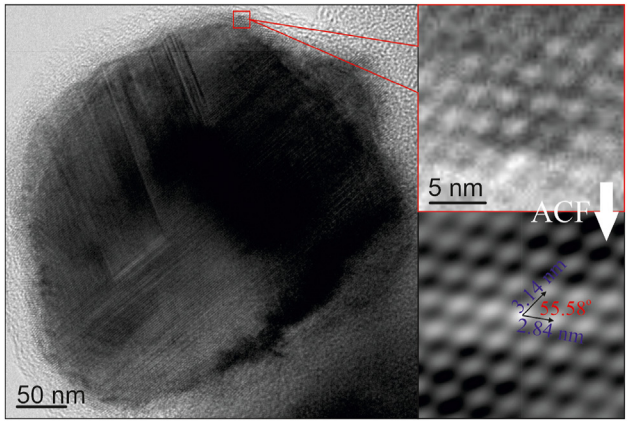

Fig. 10 – Transmission electron microscopy images of EASA-Ag NW sample (left) together with ACF processing of the sample's part image (unprocessed enlarged part of the image – upper right) with marked elemental cell vectors and angle between them (ACF processed part of the image – lower right).

In order to confirm the 2D hexagonal arrangement of mesochannels and silver nanowires in materials, we carried out the small angle X-ray diffraction with the use of an Eulerian cradle. As can be seen in Fig. 11, the XRD patterns confirm a regular 2D hexagonal pore distribution in the materials.

For the case of the EASA-COOAg 4 sample, the first Bragg reflection can be observed at $2\Theta = 2.890$deg and the second one at $2\Theta = 4.145$deg. The peaks' position is typical for reflections from the (100) and (110) planes in the hexagonal structure of the pores distributed hexagonally with a 3.53 nm distance.

The EASA-Ag NW sample presents similar features. However, the peaks' position is slightly shifted. The first Bragg peak, significantly broader than for the case uncalcined sample, can be seen at $2\Theta = 3.228$deg while the second, which is sharper, at $2\Theta = 4.449$deg. Their position reflects a

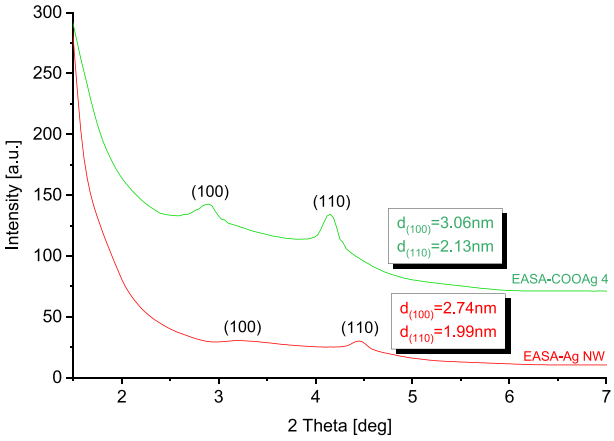

Fig. 11 – Small angle X-ray diffraction curve (OEC configuration) obtained for EASA-COOAg 4 and EASA-Ag NW thin films. The inter-planar spacings are provided above the plots.

hexagonal structure of nanowires distributed within the distance of 3.16 nm. This observation agrees with the analysis of ACF-processed TEM images: the calcined sample presents a lower interchannels' distance, which can result from the structure's shrinking during thermal processing.

4. Conclusion

In this work, we have presented a new approach for the fabrication of ultra-thin crystalline silver nanowires in vertically aligned mesoporous silica thin films. On the basis of electrochemical and microscopic research, we have established that the thermal treatment of the initial materials (mesoporous silica thin films containing silver ions anchored inside channels via propyl carbonic acid groups) resulted in the formation of continuous metallic silver nanowires localized inside pores. Obtained nanowires had a diameter of below 2 nm and presented a hexagonal $P6_3/mmc$ structure.

The spatial confinements of the silica mesopores played a crucial role in this process. The specific geometry of such silica nanoreactors allowed for the stabilization of the crystalline structure of silica nanowires with a diameter of below 2 nm. Such a geometry of crystalline structures is theoretically hardly possible since 2 nm is an edge of possible stability of hexagonal $P6_3/mmc$ structure.

The synthesis procedure presented in this work allowed for the fabrication of the unique nanocomposite, which can find an application in nanoelectronics, as a supercapacitor's electrode, for example.

Data availability

The raw data required to reproduce these findings are available to download from https://data.mendeley.com/datasets/zr66mv7577 (doi: 10.17632/zr66mv7577.1).

Declaration of Competing Interest

The authors declare that they have no known competing financial interests or personal relationships that could have appeared to influence the work reported in this paper.

Acknowledgements

Financial support for this investigation has been provided by the National Centre of Science (Grant-No: 2017/26/E/ST5/00162 (LL), 2020/37/B/ST8/03637 (LL), and 2021/43/D/ST8/00737 (ML)).

Appendix A. Supplementary data

Supplementary data to this article can be found online at https://doi.org/10.1016/j.jmrt.2023.05.029.

REFERENCES

[1] Zhou P, Yao L, Chen K, Su B. Crit Rev Anal Chem 2020;50:424–44.
[2] Walcarius A. Acc Chem Res 2021;54:3563–75.
[3] Innocenzi P. Chem Sci 2022;13:13264–79.
[4] Walcarius A, Sibottier E, Etienne M, Ghanbaja J. Nat Mater 2007;6:602–8.
[5] Goux A, Etienne M, Aubert E, Lecomte C, Ghanbaja J, Walcarius A. Chem Mater 2009;21:731–41.
[6] Teng Z, Zheng G, Dou Y, Li W, Mou C-Y, Zhang X, et al. Angew Chem Int Ed 2012;51:2173–7.
[7] Rafiee M, Karimi B, Farrokhzadeh S, Vali H. Electrochim Acta 2013;94:198–205.
[8] Vilà N, Ghanbaja J, Aubert E, Walcarius A. Angew Chem 2014;126:2989–94.
[9] Laskowska M, Pastukh O, Fedorchuk A, Schabikowski M, Kowalczyk P, Zalasiński M, et al. Int J Mol Sci 2020;21:8137.
[10] Fedorchuk A, Laskowska M. Mater Proc 2020;4:66.
[11] Fedorchuk A, Walcarius A, Laskowska M, Vila N, Kowalczyk P, Cpałka K, et al. Int J Mol Sci 2021;22:7505.
[12] Martin CR. Chem Mater 1996;8:1739–46.
[13] Lai M, Riley DJ. J Colloid Interface Sci 2008;323:203–12.
[14] Mohamed NA, Han Y, Hector AL, Houghton AR, Hunter-Sellars E, Reid G, et al. Langmuir 2022;38:2257–66.
[15] Bartlett PN, Beanland R, Burt J, Hasan MM, Hector AL, Kashtiban RJ, et al. Nano Lett 2018;18:941–7.
[16] Ramírez A, Gacitua M, Ortega E, Díaz F, del Valle M. Electrochem Commun 2019;102:94–8.
[17] del Valle MA, Gacitúa M, Díaz FR, Armijo F, del Río R. Electrochem Commun 2009;11:2117–20.
[18] Ullah W, Herzog G, Vilà N, Walcarius A. Faraday Discuss 2022;233:77–99.
[19] Del Valle M, Hernández L, Ramírez A, Díaz F. Ionics 2017;23:191–9.
[20] Ai Y, Smida H, Ghilane J, Vilà N, Ghanbaja J, Walcarius A, et al. Sci Rep 2017;7:1–9.
[21] Kim Y-T, Han JH, Hong BH, Kwon Y-U. Adv Mater 2010;22:515–8.
[22] Lu L, Zhou L, Chen J, Yan F, Liu J, Dong X, et al. ACS Nano 2018;12:12673–81.
[23] Laskowska M, Kityk I, Pastukh O, Dulski M, Zubko M, Jedryka J, et al. Microporous Mesoporous Mater 2020;306:110435.
[24] Walcarius A. Chem Soc Rev 2013;42:4098.
[25] Vilà N, Andreé E, Ciganda R, Ruiz J, Astruc D, Walcarius A. Chem Mater 2016;28:2511–4.
[26] Laskowski Ł, Laskowska M, Vila N, Schabikowski M, Walcarius A. Molecules 2019;24:2395.
[27] Losch P, Huang W, Goodman ED, Wrasman CJ, Holm A, Riscoe AR, et al. Nano Today 2019;24:15–47.
[28] Lee H, Kim C, Yang S, Han JW, Kim J. Catal Surv Asia 2011;16:14–27.
[29] Wu Y, Wang D, Li Y. Chem Soc Rev 2014;43:2112–24.
[30] Zhang M, Zou Y, Zhou X, Yan F, Ding Z. Front Chem 2022;10 [year].
[31] Lu M. Supercapacitors: materials, systems, and applications. John Wiley & Sons; 2013.
[32] Yu A, Chabot V, Zhang J. Electrochemical supercapacitors for energy storage and delivery: fundamentals and applications. CRC Press; 2013.
[33] Safaei A, Shandiz MA. Phys E Low-dimens Syst Nanostruct 2009;41:359–64.
[34] Nečas D, Klapetek P. Open Phys 2012;10:181–8.
[35] Laskowska M, Kityk I, Dulski M, Jedryka J, Wojciechowski A, Jelonkiewicz J, et al. Nanoscale 2017;9:12110–23.

[36] Mysen B, Frantz J. Contrib Mineral Petrol 1994;117:1–14.
[37] Ginter D, Went G, Bell A, Radke C. Zeolites 1992;12:733–41.
[38] Doyle CA, Vickers TJ, Mann CK, Dorsey JG. J Chromatogr A 1997;779:91–112.
[39] Lin-Vien D, Colthup NB, Fateley WG, Grasselli JG. The handbook of infrared and Raman characteristic frequencies of organic molecules. Elsevier; 1991.
[40] Krishnan K. Proc Indian Acad Sci Sect A 1961:151–67.
[41] Dendramis A, Schwinn E, Sperline R. Surf Sci 1983;134:675–88.
[42] Silverstein RM, Bassler GC. J Chem Educ 1962;39:546.
[43] Thompson WR, Pemberton JE. Anal Chem 1994;66:3362–70.
[44] Walrafen G. J Chem Phys 1975;62:297–8.
[45] Martina I, Wiesinger R, Jembrih-Simbürger D, Schreiner M. E-Preserv Sci 2012;9:1–8.
[46] Kai S, Chaozhi W, Guangzhi X. Spectrochim Acta Mol Spectrosc 1989;45:1029–32.
[47] Laskowski Ł, Laskowska M, Dulski M, Zubko M, Jelonkiewicz J, Perzanowski M, et al. Microporous Mesoporous Mater 2019;274:356–62.
[48] Courty A, Mermet A, Albouy P, Duval E, Pileni M. Nat Mater 2005;4:395–8.
[49] Duval E, Mermet A, Courty A, Albouy P, Pileni M. Phys Rev B 2005;72:085439.
[50] Barón-Jaimez J, Joya M, Barba-Ortega J. J Phys Conf 2013:012023.
[51] Sinha A, Sharma BP. Bull Mater Sci 2005;28:213–7.